Investigation on the undrained shear strength of loose sand with added materials at various mean diameter ratios

Zhehao Zhu, Feng Zhang, Jean-Claude Dupla, Jean Canou, Evelyne Foerster

Investigation on the undrained shear strength of loose sand with added materials at various mean diameter ratios

Zhehao Zhu[a], Feng Zhang[a*], Jean-Claude Dupla[a], Jean Canou[a], Evelyne Foerster[b]

[a] Ecole des Ponts ParisTech, Laboratoire Navier/CERMES, 6-8 av. Blaise Pascal, 77455 Marne La Vallée cedex 2, France

[b] Commissariat à l'énergie Atomique, DEN, DANS, DM2S, Université Paris-Saclay, F-91191 Gif-sur-Yvette, France

***Corresponding Author:**
Feng Zhang
Ecole des Ponts ParisTech
Laboratoire Navier/CERMES, 6-8 av. Blaise Pascal, 77455 Marne La Vallée cedex 2, France
Email: feng.zhang@enpc.fr

Abstract

This study aims to investigate the undrained shear strength of sand with added materials at different mean diameter ratios D_{50}/d_{50} (D_{50} and d_{50} respectively represent the mean diameter of host sand and added materials) in loose state by performing a series of undrained triaxial tests. For this purpose, a very low density index of sand matrix I_{Dmat} equaling to 0.00 was employed and the fines of C500 silt, Illite and Speswhite with distinct mean grain sizes were respectively added into the host HN31 sand at different contents F_c (5%, 10% and 15%). For comparison and further analysis, undrained triaxial tests were also carried out on Sand-Sand mixtures, created by adding the HN31 sand into the host HN31 sand at F_c of 5%, 10%, 14% and 18.7%. Results showed that, for low value D_{50}/d_{50} (e.g., 1 for Sand-Sand), the undrained shear strength S_u increased as F_c increased, which might be attributed to the increase of occlusal friction, and in that case the sliding of host sand became difficult. By contrast, in the case of higher value D_{50}/d_{50} (e.g., 58.33 for Sand-C500, 159.09 for Sand-Illite and 500 for Sand-Speswhite), S_u decreased as F_c increased. This was explained by the fact that, with increase of F_c, the quantity of added materials with small size increased, and in that case the sliding of host sand became easy. A critical value of D_{50}/d_{50} (14.5) was thus deduced, which theoretically verified the negligible effect of F_c on S_u. Furthermore, for sand mixed with fines (e.g., C500 silt, Illite and Speswhite clays), F_c has an insignificant effect on the peak value of Δu_{max}, while the increase of D_{50}/d_{50} facilitated the generation of excess pore water pressure after reaching about Δu_{max}. These findings provided useful information for analyzing the mechanical behaviour of sand with added materials in geotechnical practice.

Keywords: Loose sand; Added materials; Undrained shear strength; Mean diameter ratio

1. Introduction

There has been abundant evidence that the undrained shear strength of loose sandy soil is one of the key issues when subjected to seismic loading. Due to the rapid build-up of excess pore water pressure, loose sandy soil could undergo a transient loss of shear strength and behave as a liquid, resulting in catastrophic consequences to geotechnical structures and foundations. A sound understanding of clean sand has been already acquired since two destructive earthquakes occurred in United States and Japan in 1964: the Alaska earthquake [1] and the Niigata earthquake [2]. However, a large number of in-situ investigations proved that sand layer including low-percentage fines was also sensitive to liquefaction when suffering from the earthquake [3–7]. With this concern, it is of cardinal importance to study the undrained shear strength of sand with small-size inclusion (e.g., fines particles as added materials).

In the past three decades, numerous experimental investigations related to the effect of small-size inclusion on the undrained shear strength of loose sand have been reported [8-31]. However, no clear consensus was achieved and diverse views still exist as to whether the effect of fines is adverse or beneficial to undrained shear strength. In the published literature, with increasing fines content, the undrained shear strength of sand-fines mixtures could (i) increase [8–12]; (ii) decline [13–17]; (iii) firstly decrease until a certain threshold and then increase [18–22]. Efforts were made to explain the above seemingly at least controversial phenomena from the following aspects of added materials: plasticity index I_p, grain shape and gradation characteristic [23–26]. It was found that: (i) there was no specific monotonic relationship between plasticity index I_p and the shear strength, as a threshold plasticity index I_{pth} existed [23]; (ii) the sand-silt mixtures with rounded silt tended to exhibit lower shear strength, as compared with those contained angular silt [24]. However, a reversed trend was reported by Monkul [25] that the angular nature of silt made the sandy samples more prone to lose shear strength; (iii) the gradation characteristic had a significant effect on the overall soil response that the liquefaction resistance of silty sand generally decreased with increasing coefficient of uniformity [26]. Recently, the average size of silt grains relative to that of host sand has been repeatedly proved to be an important factor influencing the mechanical behaviour of sand-fine mixtures [27–31]. Unfortunately, these studies [27–31] only focused on the silt being as the added materials, and the

corresponding size range (5-75 μm) was comparatively narrow in most instances, rendering the complete conclusion to be drawn difficult. To the authors' knowledge, the effect of average size of added materials on the mechanical response of sandy samples remains an open issue, and further investigation is still needed.

In this study, emphasis was put on the effect of mean diameter of added materials on the undrained shear strength of host sand matrix by performing a series of undrained triaxial compression test. For this purpose, three types of fines (C500 silt, Illite and Speswhite clays) with distinct mean diameters were respectively added into the host HN31 sand at different contents in a very loose state. For comparison and further analysis, the triaxial tests were also carried out on Sand-Sand mixtures, created by adding the HN31 sand into the host HN31 sand at different contents. Furthermore, the hydraulic conductivity tests were also directly determined in the triaxial apparatus, allowing relatively satisfactory interpretation of the evolution of excess pore water pressure. From a practical point of view, the identified mechanism in this study is also helpful when further analyzing the case in cyclic triaxial tests for liquefaction resistance.

2. Materials and method

2.1. Physical properties of test materials

The host sand used in this study is a poorly graded Hostun 31 sand (HN31), which is characterized by uniform sub-angular grains and extensively used in many laboratories in Europe. The added materials were respectively HN31 sand (the same material as the host HN31 sand), C500 (a non-plastic fine silt powder), Illite Arvel (a plastic clay of Illite mineralogical content) and Speswhite (a plastic clay of Kaolinite-mineralogical content). Their physical properties are listed in Table 1. The specific gravity (G_s) of the test materials is found to be the same, which is 2.65. For Illite Arvel and Speswhite, the plasticity indexes were determined using the French Standard NF P 94-051, which were respectively equal to 34 and 30. It is worth noting that, for C500 silt, it was difficult to obtain a standard roller determining its plasticity, being reasonably considered as NP (Non-Plastic) fines. The grain size distribution curve of non-plastic materials (e.g., HN31, C500 in Fig. 1) was measured by laser diffraction method. A particle could scatter the light at a certain angle and intensity while passing through a laser beam, allowing the determination of its grain size [24]. The grain size distribution curve of plastic fines (e.g., Illite) was determined by settlement analysis method (see Fig. 1) since it was more accurate for finer cohesive soil (< 80 μm). The principle of the method is to measure the sedimentation rate of soil particles in a static liquid that related to its equivalent particles diameter. Note that the curve of Speswhite was measured and checked by Muhammed [32]. It appears that, for host HN31 sand, the mean diameter is 350 μm, while for C500, Illte Arvel and Speswhite, the mean diameters are 6 μm, 2.2 μm and 0.7 μm, respectively. These four added materials (HN31 sand, C500 silt, Illte Arvel and Speswhite clays) into the host HN31 sand create the mean diameter ratio (D_{50}/d_{50}) of 1, 58.33, 159.09 and 500, respectively. It is worth noting that the D_{50} refers to the mean diameter of the host HN31 sand, while the d_{50} refers to the mean diameter of the added materials.

In most of the existing references, the constant global void ratio was considered (see Fig. 2a): the addition of small grains (e.g., fines) systematically reduced the quantity of host sand to keep the global void ratio unchanged, allowing the preparation of tested samples with high content of added

materials (e.g., fines). The constant global void ratio considered also led to the reduction of quantity of the host sand, and made the overall response of soil sample change from the dominance of host sand to that of added materials (e.g., fines) [33,34]. However, the density index of sand matrix [35] I_{Dmat} was considered in this study (see Fig. 2b). The clear benefit was that for each series of undrained triaxial compression test, the quantity of sand matrix was kept exactly unchanged, irrespective of the varying content of added materials (e.g., fines). In that case, the skeleton of the sample was greatly sand-prevailing but polluted by a small amount of added materials (e.g., fines), which is accord with the real field situation [5,36]. A low density index of sand matrix I_{Dmat} equaling to 0.00 was employed (I_{Dmat} = (e_{max}-e_{mat})/(e_{max}-e_{min}), where e_{mat} is the void ratio of sand matrix, e_{max} and e_{min} represent the maximum and minimum void ratios of clean sand [37], respectively). The content of added materials F_c was thus defined as the dry mass of added materials divided by that of sand matrix (m_{add}/m_{sand}). Three low-percentage of F_c = 5%, 10% and 15% were selected for the added materials of C500, Illite and Speswhite, as well as four low-percentage of F_c = 5%, 10%, 14% and 18.7% for the added materials of HN31 sand, as the skeleton of the sample was dominated by the sand-sand contacts in that case ([9,38,39]). For comparison, the total content of added materials F_c^T (the ratio of the mass of added materials to the total mass of composite sandy mixture) are also given in Table 2.

2.2. Reconstitution method

As for reclaimed binary mixture, the major challenge in reconstitution step is the homogeneity of composite soil mixture. First attempts had been made to apply moist tamping technique. However, a non-uniform mixture was created through the observations of small aggregates since plastic fines (e.g., Speswhite) stuck together even with a small amount of water. To overcome this problem, dry tamping technique was thus adopted. In this method, two materials were firstly mixed by shaking in an enclosed container. Then, all mixtures were divided into 10 parts and each part was carefully introduced into a split mould by a spoon (see Fig. 3a). The clear benefit of spooning was: (i) to reduce the drop distance as much as possible to achieve such a loose state I_{Dmat}=0.00; (ii) to avoid initial segregation between coarse and small-size grains during freefall. Finally, the sample with 10 cm in

diameter and 20 cm in height was created. During this process, the horizontality was checked by a horizontal rule (see Fig. 3b).

2.3. Triaxial test program

The test program is summarized in Table 2. In test TM1, once the specimen had been formed, the top triaxial cap was placed and sealed with two O-rings. A vacuum of about 20 kPa was applied to reduce possible disturbances while removing the split mould, as well as to check the leakage of membrane. After ensuring that the latex membrane was not defective, the confining pressure was increased to 20 kPa to maintain the sample before cancelling the inside vacuum and increased to 100 kPa for the saturation stage. Carbon dioxide (CO_2) was then purged into the dry sample for about 15 mins under a pressure of about 15 kPa to evacuate air bubbles, followed by injecting de-aired water to saturate the sample. It is worth noting that the flux of de-aired water was minimized to avoid the possible migration of added materials passing through the sample. Prior to applying back pressure, the falling head permeability test was performed under a constant confining pressure of 100 kPa: an initial water head (about 1 m height) was applied in the bottom drainage and the top base of the sample was kept at atmospheric pressure. Based on the water head loss recorded at a fixed time, the hydraulic conductivity k could be determined according to the variable water head method using Darcy's law. Afterwards, the back pressure and confining pressure were increased alternatively in equal incremental steps of 20 kPa until they were respectively equal to 200 kPa and 300 kPa. The Skempton's B value ($B = \Delta u/\Delta\sigma_{conf}$, the variation of excess pore water pressure divided by that of confining pressure) was checked, normally a value higher than 0.98 was achieved. This criterion was believed to be sufficiently high for full saturation of sandy soils. Finally, the sample was sheared under undrained condition at a constant rate of 0.5%/min. This rate was believed to be low enough to allow the equilibrium of pore water pressure, which was also carefully checked by the measurements at the base and top of the samples. The tests ended after the axial strain reached 20%. The similar procedures were also applied to tests TM2-TM15. Note that the hydraulic conductivity test was only performed on sand-fines samples TM5-15.

All the tests were carried out at a controlled ambient temperature 20 ± 1 ºC.

3. Experimental results

3.1. Permeability tests

Fig. 4 presents the variation of hydraulic conductivity k with F_c for TM5-15 mixtures at different contents before shearing. It is observed that, for Sand-C500 mixtures, the k decreased at a fast rate when F_c was smaller than 5%. By contrast, in the case of F_c higher than 5%, the decline tendency of k with F_c became small. While for Sand-Illite and Sand-Speswhite mixtures, the k almost linearly decreased as F_c increased. Moreover, at the same F_c, the highest k values were identified for Sand-Speswhite mixtures, the lowest ones were detected for Sand-C500 mixtures and the values in-between for Sand-Illite mixtures. The results here suggest that even at the identical fines content, the clogs of main pathway for water (e.g., the connectivity of inter-sand voids) for the three materials were not the same: the severest extent was expected for the addition of C500 (NP fines), the fewest one was expected for the addition of Speswhite (I_p=30), and the one in-between for Sand-Illite mixtures (I_p=34). Considering that there is no clear monotonic relationship between hydraulic conductivity and plasticity of added materials, the above phenomenon might be attributed to the fact that the main pathway for water formed by host sand became increasingly clogged with the increase of added grains size ($d_{50\text{-C500}}$> $d_{50\text{-Illite}}$> $d_{50\text{-Speswhite}}$).

3.2. Triaxial tests

Fig. 5 shows the evolutions of deviator stress (q) with axial strain (ε_a) in the cases of two parallel samples for Sand-C500 mixture, as well as for Sand-Speswhite mixture. It can be observed that for Sand-C500 mixture, the two curves were almost the same, exhibiting a satisfactory repeatability of the test. The similar phenomenon was also identified for Sand-Speswhite mixture. This confirms that the

188 protocol adopted in the experimental program is pertinent and repeatable with respect to mixture
189 homogeneity.

190 Fig. 6(a)-(b) presents the deviator stress/excess pore water pressure ($q/\Delta u$) against axial strain
191 (ε_a) in the cases of Sand-Sand mixtures (F_c = 5%, 10%, 14% and 18.7%). It appears from Fig. 6 (a)
192 that: (i) for F_c = 5%, the deviator stress q linearly increased with ε_a (ε_a < 0.5%) and then kept almost
193 constant till ε_a = 2%. Afterwards, a strain hardening tendency was noted. Finally, the q slightly
194 increased till the end of test; (ii) for F_c = 10%, 14% and 18.7%, a dramatic increase in q was observed
195 at the beginning; then q began to decrease after reaching a peak deviator value (q_{max}). Finally, the
196 deviator stress reached the critical state, exhibiting a strong dilatant behavior; (iii) the F_c had a
197 significant effect on the q_{max}, and q_{max} increased as the F_c increased. The excess pore water pressure
198 characterized in Fig. 6(b) shows that: (i) a short-lived contractive behaviour occurred, followed by a
199 large dilatant phase range; (ii) cavitation was achieved in all cases and Δu decreased as the F_c
200 increased.

201 Fig. 6(c)-(d) describes the evolution of $q/\Delta u$ with ε_a in the cases of Sand-C500 mixtures at F_c =
202 5%, 10% and 15%. It can be noticed from Fig. 6(c) that q quickly increased in the range of ε_a smaller
203 than 0.5%, then slowly increased till the end of tests (ε_a = 20%). In addition, the F_c has an ignorable
204 effect on the q when ε_a was smaller than about 2%. By contrast, in the case of ε_a higher than 2%, the
205 dominant role of F_c was identified by the remarkable weakening in q. As for Δu in Fig. 6(d), it appears
206 that Δu quickly increased till ε_a equaling to 2%; then decreased until the end of test (ε_a = 20%).
207 Moreover, F_c had an insignificant effect on the Δu when the ε_a was smaller than about 2%. On the
208 contrary, in the case of ε_a higher than 2%, F_c became prevailing, and Δu increased as F_c increased,
209 suggesting that the increase of F_c encouraged the generation of excess pore water pressure.
210 Concerning Sand-Illite and Sand-Speswhite mixtures, the similar variation tendency of deviator
211 stress/excess pore water pressure curves were observed that: with the increase of F_c, the deviator stress
212 decreased and the corresponding excess pore water pressure increased when ε_a was higher than about
213 2%, as shown in Fig. 6(e)-(h). This is consistent with the results reported by Jradi [10], who performed

214 the monotonic and cyclic triaxial tests on NE34 Sand-Speswhite mixtures, and found that the deviator
215 stress decreased as the plastic fines content increased.

216 Fig. 7(a)-(b) displays the evolution of $q/\Delta u$ for three mixtures at F_c equaling to 5%. The curves in
217 Fig. 7(a) show that for Sand-C500 mixture with low D_{50}/d_{50} (58.33), the gain in q with respect to ε_a
218 was steadily increasing. However, for Sand-Speswhite with higher D_{50}/d_{50} (500), different phenomena
219 were observed: the q almost linearly increased with ε_a ($\varepsilon_a < 0.5\%$), then slightly decreased till
220 ε_a equaling to 2%. Afterwards, the q increased until the end of test (ε_a = 20%). In addition, D_{50}/d_{50} had
221 an insignificant effect on q when the ε_a was smaller than about 0.5%. On the contrary, in the case of ε_a
222 higher than 0.5%, D_{50}/d_{50} became prevailing, and the q decreased as the D_{50}/d_{50} increased, suggesting
223 that the increase of D_{50}/d_{50} decreased the shear strength. The results identified in Fig. 7(b) show that: (i)
224 Δu quickly increased with ε_a till ε_a equaling to 2%; then decreased with ε_a until the end of test (ε_a
225 =20%); (ii) the D_{50}/d_{50} had an insignificant effect on the Δu when the ε_a was smaller than about 0.5%.
226 By contrast, when ε_a was higher than 0.5%, the Δu increased as the D_{50}/d_{50} increased, suggesting that
227 the increase of D_{50}/d_{50} facilitated the generation of excess pore water pressure. The similar phenomena
228 were identified for Sand-C500, Sand-Illite and Sand-Speswhite mixtures at F_c=10% (Fig. 7c-d) and 15%
229 (Fig. 7e-f).

230 For further analyzing the effect of D_{50}/d_{50}, the results in terms of undrained shear strength S_u
231 ($q_{max}/2$) versus F_c for Sand-Sand (D_{50}/d_{50} = 1), Sand-C500 (D_{50}/d_{50} = 58.33, NP fines), Sand-Illite
232 (D_{50}/d_{50} = 159.09, $I_{p,Illite}$=34) and Sand-Speswhite (D_{50}/d_{50} = 500, $I_{p,Speswhite}$=30) mixtures are
233 schematized in Fig. 8(a). The results in terms of excess pore water pressure ratio r_u ($\Delta u_{max}/\dot{\sigma}_c$, the peak
234 value of excess pore water pressure divided by the effective confining pressure) versus D_{50}/d_{50} for
235 Sand-C500 (D_{50}/d_{50} = 58.33, NP fines), Sand-Illite (D_{50}/d_{50} = 159.09, $I_{p,Illite}$=34) and Sand-Speswhite
236 (D_{50}/d_{50} = 500, $I_{p,Speswhite}$=30) mixtures are shown in Fig. 8b. Note that Δu_{max} is almost the same for
237 Sand-C500 (about 64 kPa, see Fig. 6d), Sand-Illite (about 76 kPa, see Fig. 6f), Sand-Speswhite (about
238 84 kPa, see Fig. 6h) mixtures at different F_c, while for Sand-Sand mixture, the excess pore water
239 pressure changed with F_c (see Fig. 6b). Therefore, the result of Sand-Sand mixture was not presented
240 in Fig. 8(b). It appears from Fig. 8(a) and Fig. 8(b) that: (i) for a given content of added materials, the

undrained shear strength decreased with the increase of D_{50}/d_{50}; (ii) for Sand-Sand mixture of D_{50}/d_{50}=1, S_u increased as F_c increased, while a reversed phenomenon was observed for higher D_{50}/d_{50}, and S_u decreased as F_c increased; (iii) r_u monotonically increased as D_{50}/d_{50} increased (see Fig. 8b), indicating that the increase of D_{50}/d_{50} enabled the excess pore water pressure to be rapidly developed. To further analyze, the slopes ($\Delta S_u/\Delta F_c$) were determined from the curves of S_u versus F_c, and the values are listed in Table 3. It was found that $\Delta S_u/\Delta F_c$ monotonically decreased while D_{50}/d_{50} altering from 1 to 500 (see Fig. 8a and Table 3). The results here suggest that the combined dimensionless parameter (D_{50}/d_{50}) linking to relative grains size shows a good performance to describe the mechanical behaviour since it is able to express the coupled influence of sand and added materials.

It is worth noting that attempts were also made to measure the grading curve for plastic fines (e.g., Illite) for the determination of d_{10}. However, after applying the sedimentation analysis method for Illite, the grain size distribution curve identified in Fig. 1 shows that it was extremely difficult to precisely measure the grain size lower than 2 μm, leading to the unreliable determination of d_{10}. This also renders the further interpretation based on the parameters of D_{10}/d_{10} and C_u (d_{60}/d_{10}) difficult in this study.

4. Discussion

4.1. Effect of mean diameter ratio

As for coarse sand with added materials at low-percentage F_c (dominance of host sand), the overall skeleton of composite soil is constituted by coarse sand matrix [39]. The role of added materials depends on the grain size with respect to that of the host sand. For grain size being close to that of the host sand (see Fig. 9a), the addition of materials increased the occlusal friction represented by the reciprocal constraint of adjacent sand on their relative movements. Consequently, the sliding of sand became difficult, leading to the increase of undrained shear strength. By contrast, in the case of grain size much smaller than that of the host sand (see Fig. 9b), small-size grains have two main positional tendencies during the deposition process, as mentioned by Monkul [25]: (i) they could possibly be

accommodated into inter-sand voids space formed by host sand, and the small-size grains could be viewed as inactive. In that case, they are free to move inside the inter-sand voids existed in such a loose state (I_{Dmat}=0.00), and do not directly participate in global force at least in the small range of F_c (dominance of host sand). This is consistent with the conclusion drawn by Finn [40] that small-size grains completely accommodated within the voids produced by host sand made no contribution to the mechanical response of composite soil; (ii) they could possibly be located between contacts points of host sand by separating them, and the addition of smaller grains loosened the packing of host sand [41], facilitating the relative sliding of host sand.

As mentioned previously, for Sand-Sand mixtures, the grain size of added materials was equal to that of host sand, and in that case, the increase in F_c corresponded to the increase of occlusal friction between sand-sand contacts, leading to the increase of S_u. This is also consistent with the results obtained by Wang [39], who performed the monotonic triaxial tests on six kinds of soil samples with different volumetric contents of coarse grains (D_{50}/d_{50}<1 of Sand-Ballast mixtures), and found that the shear strength increased as the volumetric contents of coarse grains increased. Whereas, the mean diameter of C500, Illite and Speswhite are much smaller than that of host sand, making the mean diameter ratio D_{50}/d_{50} significantly greater than 1. In that case, the sliding effect became apparent, resulting in the easy sliding of sand in such a loose state of I_{Dmat} = 0.00. This explained the decrease of undrained shear strength S_u with F_c for Sand-C500, Sand-Illite and Sand-Speswhite mixtures observed in Fig. 8(a). Meanwhile, for a given F_c, the increase of D_{50}/d_{50} corresponded to the decreasing diameter of added materials, leading to the increasing quantity of added materials. And in that case, the sliding of sand became relatively easier. This explained the decrease of undrained shear strength with the increase of D_{50}/d_{50}, as shown in Fig. 8(a).

According to the above analysis, it could be logically deduced that there essentially exists a critical value of D_{50}/d_{50}, at which F_c has a negligible effect on the S_u of mixtures. Following up this logic, this critical value was deduced from the $\Delta S_u/\Delta F_c$ versus D_{50}/d_{50} (see Table 3), at which the $\Delta S_u/\Delta F_c$ was equal to 0. A value of 14.5 was obtained from Fig. 10, which theoretically verified the negligible effect of F_c on the S_u. In that case, the effect of occlusal friction was equal to that of sliding

of sand. Thereby, when D_{50}/d_{50} was smaller than 14.5, the addition of materials corresponded to the global increase of occlusal friction, and the sliding of sand became difficult, leading to the increase of shear strength. By contrast, in the case of D_{50}/d_{50} higher than 14.5, the sliding of sand became easy; as a result, the shear strength decreased as F_c increased. It is worth noting that this critical value (14.5) was determined from four points, more points are needed to clarify this aspect.

As regards the results of Δu versus ε_a, it is observed from Sand-Sand mixtures that: the peak value of Δu decreased as the F_c increased (see Fig. 6b). This might be attributed to the fact that, with the increase in F_c, the clog of main pathway for water increased. And in that case, the generation of pore water pressure was inhibited during shearing. Following up this logic, the similar phenomenon should be also observed for Sand-C500, Sand-Illite and Sand-Speswhite mixtures (the peak value of Δu should decrease as the F_c increased), as the clog extent of main pathway for water increased, characterized by the decrease in hydraulic conductivity k with F_c (see Fig. 4). However, the results identified in Fig. 6(d), (f), (h) did not support this reasoning: F_c seemed to have an insignificant effect on this peak value. This might be attributed to the following two factors: (i) although the hydraulic conductivity k was determined prior to shearing, it still could be supposed to be representative in the small range of ε_a where Δu_{max} appeared. Therefore, with the increase of F_c, clog effect inhibiting the generation of pore water pressure was confirmed by Fig. 4 that k decreased as F_c increased; (ii) the addition of relatively small-size fines such as C500, Illite and Speswhite into host sand matrix enhanced the contraction phenomenon, leading to the generation of more pore water pressure, as mentioned previously. Thereby, the insignificant effect of F_c on the peak value of Δu_{max} identified in Fig. 6(d) for Sand-C500, in Fig. 6(f) for Sand-Illite and in Fig. 6(h) for Sand-Speswhite mixtures combined the above two factors. As regards the increase of r_u with D_{50}/d_{50} (see Fig. 8b), it might be attributed to the sliding effect that the contraction phenomenon was enhanced, as mentioned previously. It might be also attributed to the less clog extent of main pathway for water, justified by the increasing hydraulic conductivity with D_{50}/d_{50} (see Fig. 4).

4.2. Effects of other indicators

It is worth noting that in addition to the grain size (represented by D_{50}/d_{50}), other factors such as plasticity index I_p and grain shape may also affect the mechanical response [23–26,42]. General speaking, the plasticity index I_p of added clayey fines (especially for the highly expansive clay) should have a significant effect on the hydro-mechanical behaviour of sandy mixtures. However, the results observed in this study suggest that I_p is not a good indicator for analyzing the effect of added materials on undrained shear strength, at least for the three added materials with low I_p that were considered in this study (C500, Illite and Speswhite) since the comparatively small difference in plasticity indexes between Speswhite ($I_{p,Speswhite}$=30) and Illite ($I_{p,Illite}$=34) could not legitimately explain such a significant discrepancy in mechanical responses (see Fig. 8a and Fig. 8b). This is also consistent with the results obtained by Park [43], who performed the triaxial tests on loosely prepared sandy deposits with the addition of fines materials of distinct plasticity indexes (e.g., from I_p=8 of silt to I_p=377 of bentonite employed), and found that although liquefaction resistance of samples indeed decreased with the increase of plasticity, however, the observed tendency was not obvious. As regards the effect of the grain shape of added materials, it may depend on the grain size (represented by D_{50}/d_{50}): (i) for Sand-Sand or Sand-Silt mixtures with low value of D_{50}/d_{50}, the angularity of the added materials might play an important role because this physical parameter directly determines the occlusal level of overall soil matrix [37]; (ii) on the contrary, for sand-fines mixtures especially with the addition of clayey materials (e.g., Illite and Speswhite), one might expect an ignorable effect of shape characteristic since the added materials are enough smaller than the host sand forming the overall soil matrix. Indeed, Carraro [44] reported an increase/decrease of both peak and critical-state friction angle by performing triaxial test on host sand with the addition of non-plastic silt/plastic kaolinite clay, and pointed out that more angular non-plastic silt tended to increase undrained shear strength during shearing, whilst an opposite phenomenon was observed for more rounded clay particles. This is also consistent with the results obtained by Yang [24], who performed a series of triaxial tests on sand-silt mixture, and found that the sand-silt mixtures with angular silt tended to exhibit higher shear strength, as compared with that for sand-silt mixtures with the addition of rounded silt. And they attributed this phenomenon to

the fact that rounded fines could further facilitate the sliding in the loose state. However, a reversed trend was reported by Monkul [25] that the angular nature of silt made the sandy samples more prone to lose shear strength. Like the effect of plasticity index of the added materials on the undrained shear strength (as mentioned previously), no common conclusion was achieved in terms of the effect of grain shape. Further studies are thus needed to clarify these points. However, it is believed that the mechanism identified in this study in the large range of D_{50}/d_{50} (from 1 to 500) would be still applicable.

5. Conclusions

In this study, the effect of mean diameter ratio D_{50}/d_{50} on the undrained shear strength of a loose sand matrix (I_{Dmat}=0.00) was investigated by respectively adding three fines (with different mean diameter ratios D_{50}/d_{50}) at content of 5%, 10% and 15% (by mass), and by performing a series of triaxial compression tests under undrained condition. For further comparison and analysis, the triaxial tests were also performed on Sand-Sand mixtures at four contents of 5%, 10%, 14% and 18.7%. The results obtained allow the following conclusions to be drawn.

The evolution of S_u and r_u proved that D_{50}/d_{50} could serve as a pertinent indicator to evaluate the undrained shear strength of sand with added materials since it considered the coupled characteristics between two materials. For low value D_{50}/d_{50} (e.g., 1 for Sand-Sand mixtures), S_u increased as F_c increased, which might be attributed to the increase of occlusal friction, similar to the densification effect. On the contrary, for higher value D_{50}/d_{50} (e.g., 58.33 for Sand-C500, 159.09 for Sand-Illite and 500 for Sand-Speswhite), the undrained shear strength S_u decreased as F_c increased. In fact, the increase of D_{50}/d_{50} corresponded to decreasing diameter of added materials. In that case, the corresponding quantity of added materials increased, leading to the easy sliding of sand. A critical value of D_{50}/d_{50} (14.5) was thus deduced, which theoretically verified the negligible effect of F_c on S_u. Moreover, for sand with fines (C500 silt, Illite and Speswhite) mixtures, the increase of F_c had insignificant effect on the peak value of Δu_{max}, while the increase of D_{50}/d_{50} facilitated the generation of excess pore water pressure after reaching about Δu_{max}.

From practical points of view, the results obtained in this study are very helpful for analyzing the undrained shear strength in loose state, as well as for designing the geotechnical structures. Indeed, as for quasi-binary mixture, when the D_{50}/d_{50} of mixtures is higher than the critical value, the shear strength decreases as the F_c increases. Only when the D_{50}/d_{50} becomes lower than the critical value, the undrained shear strength increases as the F_c increases, thus the resistance to liquefaction increases.

Acknowledgments

The authors acknowledge the support of the geotechnical laboratory of Ecole des Ponts ParisTech. The finical support provided by the research sponsors through ANR ISOLATE is gratefully acknowledged.

References

[1] Wyss M, Brune J. The Alaska earthquake of 28 March 1964: A complex multiple rupture. Bull Seismol Soc Am 1967;57:1017–23.

[2] Ishihara K, Koga Y. Case Studies of Liquefaction In the 1964 Niigata Earthquake. Soils Found 1981;21:35–52.

[3] Ohsaki Y. Effects of Sand Compaction on Liquefaction During The Tokachioki Earthquake. Soils Found 1970;X. https://doi.org/10.1061/ASCE1090-0241200312911.

[4] Shengcong F, Tatsuoka F. Soil Liquefaction During Haicheng and Tangshan Earthquake in China; A Review. Soils Found 1984;24:22–9.

[5] Tokimatsu K, Yoshimi Y. Empirical Correlation of Soil Liquefaction Based on SPT N-Value and Fines Content. Soils Found 1983;23.

[6] Tokimatsu K, Yoshimi Y. Field correlation of soil liquefaction with SPT and grain size. F. Correlqtion Soil Liq. with SPT Grain Size, International Conferences on Recent Advances in Geotechnicql Earthquake Engineering and Soil Dynamics; 1981, p. 203–8.

[7] Seed HB, ASCE F, Idriss IM, Arango I. Case Studies of Liquefaction In the 1964 Niigata Earthquake. J Geotech Eng 1983;109:458–82.

[8] Amini F, Qi G. Liquefaction Testing of Stratified Silty Sands. J Geotech Geoenvironmental Eng 2000;126:208–17.

[9] Benahmed N, Nguyen TK, Hicher PY, Nicolas M. An experimental investigation into the effects of low plastic fines content on the behaviour of sand/silt mixtures. Eur J Environ Civ Eng 2015;19:109–28. https://doi.org/10.1080/19648189.2014.939304.

[10] Jradi L. Study of the Influence of Fine Particles on the Properties of Liquefaction of Sands. Ph.D Thesis University Paris-Est, 2018.

[11] Pitman T, Robertson P, Sego D. Influence of fines on the collapse of loose sands. Can Geotech

J 1994;31:728–39.

[12] Ni Q, Tan TS, Dasari GR, Hight DW. Contribution of fines to the compressive strength of mixed soils. Géotechnique 2004;54:561–9. https://doi.org/10.1680/geot.54.9.561.56936.

[13] Belkhatir M, Arab A, Della N, Missoum H, Schanz T. Liquefaction resistance of Chlef river silty sand: Effect of low plastic fines and other Parameters. Acta Polytech Hungarica 2010;7:119–37.

[14] Stamatopoulos CA. An experimental study of the liquefaction strength of silty sands in terms of the state parameter. Soil Dyn Earthq Eng 2010;30:662–78. https://doi.org/10.1016/j.soildyn.2010.02.008.

[15] Polito C. The Effects Of Non-Plastic and Plastic Fines On The Liquefaction Of Sandy Soils. Verginia Polytechnic Institute, 1999.

[16] Bouferra R, Shahrour I. Influence of fines on the resistance to liquefaction of a clayey sand. Gr Improv 2004;8:1–5. https://doi.org/10.1680/grim.8.1.1.36366.

[17] Ghahremani M, Ghalandarzadeh A. Effect of Plastic Fines on Cyclic Resistance of Sands. Soil Rock Behav Model 2006:406–12.

[18] Lade P, Yamamuro J. Effects of nonplastic fines on static liquefaction of sands. Can Geotech J 1997;34:918–28. https://doi.org/10.1139/t97-052.

[19] Thevanayagam S, Shenthan T, Mohan S, Liang J. Undrained fragility of clean sands, silty sands, and sandy silts. J Geotech Geoenvironmental Eng 2002;128:849–59. https://doi.org/10.1061/jggefk.

[20] Abedi M, Yasrobi SS. Effects of plastic fines on the instability of sand. Soil Dyn Earthq Eng 2010;30:61–7. https://doi.org/10.1016/j.soildyn.2009.09.001.

[21] Yang SL, Sandven R, Grande L. Instability of sand-silt mixtures. Soil Dyn Earthq Eng 2006;26:183–90. https://doi.org/10.1016/j.soildyn.2004.11.027.

[22] Xenaki VC, Athanasopoulos GA. Liquefaction resistance of sand-silt mixtures: An experimental investigation of the effect of fines. Soil Dyn Earthq Eng 2003;23:1–12. https://doi.org/10.1016/S0267-7261(02)00210-5.

[23] Papadopoulou AI, Tika TM. The effect of fines plasticity on monotonic undrained shear strength and liquefaction resistance of sands. Soil Dyn Earthq Eng 2016;88:191–206. https://doi.org/10.1016/j.soildyn.2016.04.015.

[24] Yang J, Wei LM. Collapse of loose sand with the addition of fines: The role of particle shape. Geotechnique 2012;62:1111–25. https://doi.org/10.1680/geot.11.P.062.

[25] Monkul MM, Etminan E, Şenol A. Coupled influence of content, gradation and shape characteristics of silts on static liquefaction of loose silty sands. Soil Dyn Earthq Eng 2017;101:12–26. https://doi.org/10.1016/j.soildyn.2017.06.023.

[26] Monkul MM, Etminan E, Şenol A. Influence of coefficient of uniformity and base sand gradation on static liquefaction of loose sands with silt. Soil Dyn Earthq Eng 2016;89:185–97. https://doi.org/10.1016/j.soildyn.2016.08.001.

[27] Doygun O, Brandes HG, Roy TT. Effect of Gradation and Non-plastic Fines on Monotonic and Cyclic Simple Shear Strength of Silica Sand. Geotech Geol Eng 2019;37:3221–40. https://doi.org/10.1007/s10706-019-00838-9.

[28] Belkhatir M, Arab A, Schanz T, Missoum H, Della N. Laboratory study on the liquefaction resistance of sand-silt mixtures: Effect of grading characteristics. Granul Matter 2011;13:599–609. https://doi.org/10.1007/s10035-011-0269-0.

[29] Monkul MM, Yamamuro JA. Influence of silt size and content on liquefaction behavior of sands. Can Geotech J 2011;48:931–42. https://doi.org/10.1139/t11-001.

[30] Cherif Taiba A, Belkhatir M, Kadri A, Mahmoudi Y, Schanz T. Insight into the Effect of Granulometric Characteristics on the Static Liquefaction Susceptibility of Silty Sand Soils. Geotech Geol Eng 2016;34:367–82. https://doi.org/10.1007/s10706-015-9951-z.

[31] Huang Y, Zhao L. The effects of small particles on soil seismic liquefaction resistance: current findings and future challenges. Nat Hazards 2018;92:567–79. https://doi.org/10.1007/s11069-018-3212-4.

[32] Muhammed R. Etude en chambre d'étalonnqge du frottement sol-pieu sous grands nombre de cycles. Application au calcul des fondations profonds dans les sols fins saturé. Ph.D Thesis Université Pierre et Marie Curie, 2015.

[33] Yang S, Lacasse S, Sandven R. Determination of the transitional fines content of mixtures of sand and non-plastic fines. Geotech Test J 2006;29:102–7. https://doi.org/10.1520/gtj14010.

[34] Zhu Z, Dupla J, Canou J, Foerster E. Experimental study of liquefaction resistance : effect of non-plastic silt content on sand matrix. Eur J Environ Civ Eng 2020;0:1–19. https://doi.org/10.1080/19648189.2020.1765198.

[35] El Dine BS, Dupla JC, Frank R, Canou J, Kazan Y. Mechanical characterization of matrix coarse-grained soils with a large-sized triaxial device. Can Geotech J 2010;47:425–38. https://doi.org/10.1139/T09-113.

[36] Ishihara K, Kawase Y, Nakajima M. Liquefaction characteristics of sand deposits at an oil tank site during the 1978 Miyagiken-Oki earthquake. Soils Found 1980;20:97–111.

[37] Benahmed N. Comportement mécanique d'un sable sous cisaillement monotone et cyclique: application aux phénomènes de liquéfaction et de mobilité cyclique. Ph.D Thesis Ecole Nationale Des Ponts et Chaussées, 2001.

[38] Cubrinovski M, Ishihara K. Maximum and Mimimum Void Ratio Characteristics of Sands. Soils Found 2002;42:65–78.

[39] Wang HL, Cui YJ, Lamas-Lopez F, Calon N, Saussine G, Dupla JC, et al. Investigation on the mechanical behavior of track-bed materials at various contents of coarse grains. Constr Build Mater 2018;164:228–37. https://doi.org/10.1016/j.conbuildmat.2017.12.209.

[40] Finn WD, Ledbetter RH, Wu G. Liquefaction in silty soils: design and analysis. Liq. silty soils

Des. Anal. Gr. Fail. under Seism. Cond., 1994, p. 51–76.

[41] Liu ZR, Ye WM, Zhang Z, Wang Q, Chen YG, Cui YJ. Particle size ratio and distribution effects on packing behaviour of crushed GMZ bentonite pellets. Powder Technol 2019;351:92–101. https://doi.org/10.1016/j.powtec.2019.03.038.

[42] Eseller-Bayat EE, Monkul MM, Akin Ö, Yenigun S. The Coupled Influence of Relative Density, CSR, Plasticity and Content of Fines on Cyclic Liquefaction Resistance of Sands. J Earthq Eng 2019;23:909–29. https://doi.org/10.1080/13632469.2017.1342297.

[43] Park SS, Kim YS. Liquefaction resistance of sands containing plastic fines with different plasticity. J Geotech Geoenvironmental Eng 2013;139:825–30. https://doi.org/10.1061/(ASCE)GT.1943-5606.0000806.

[44] Carraro J, Prezzi M, Salgado R. Shear Strength and Stiffness of Sands Containing Plastic or Nonplastic Fines. J Geotech Geoenvironmental Eng 2009;135(9):1169–78. https://doi.org/10.1061/(ASCE)1090-0241(2009)135.

Table and Figure

Table 1 Physical properties of test materials

Material	Mineralogical Content	D_{50} or d_{50} (μm)	e_{min}	e_{max}	G_s	I_p (-)
HN31	Sand	350	0.656	1		NP
C500	Silt	6	-	-		NP
Illite Arvel	Illite	2.2	-	-	2.65	34
Speswhite	Kaolinite	0.7	-	-		30

Table 2 Undrained triaxial test programs

Test	Added materials	F_c (1) (%)	F_c^T (2) (%)	D_{50}/d_{50}	e_{mat}	I_{Dmat}	σ'_c (kPa)
TM1	HN31 (NP)	5	4.8	1	1.00	0.00	100
TM2		10	9.1				
TM3		14	12.3				
TM4		18.7	15.8				
TM5	C500 (NP)	5	4.8	58.33			
TM6		10	9.1				
TM7		10	9.1				
TM8		15	13.0				
TM9	Illite Arvel (I_p=34)	5	4.8	159.09			
TM10		10	9.1				
TM11		15	13.0				
TM12	Speswhite (I_p=30)	5	4.8	500			
TM13		10	9.1				
TM14		10	9.1				
TM15		15	13.0				
Note	*1.* $F_c = (m_{add} / m_{sand}) \times 100\%$ *2.* $F_c^T = (m_{add} / (m_{add}+m_{sand})) \times 100\%$						

504 Table 3 Summary of undrained triaxial test results

Test	Added materials	F_c (%)	q_{max} (kPa)	S_u (kPa)	$\Delta S_u/\Delta F_c$ (kPa)	D_{50}/d_{50} (-)	Δu_{max} (kPa)	r_u (-)
TM1	HN31 (NP)	5	928	464	1374	1	70	0.7
TM2		10	1080	540			44	0.44
TM3		14	1125	562.5			35	0.35
TM4		18.7	1324	662			34	0.34
TM5	C500 (NP)	5	652	326	-670	58.33	64	0.64
TM6		10	576	288				
TM8		15	518	259				
TM9	Illite (I_p=34)	5	546	273	-870	159.09	76	0.76
TM10		10	480	240				
TM11		15	372	186				
TM12	Speswhite (I_p=30)	5	276	138	-920	500	84	0.84
TM13		10	180	90				
TM15		15	92	46				

505

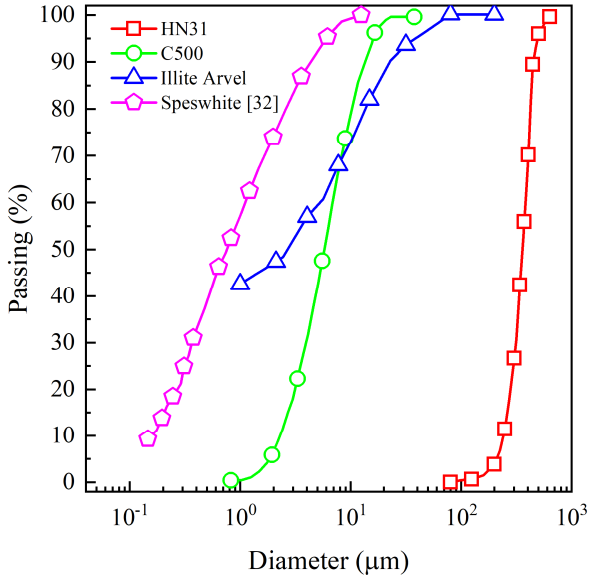

506

507 Figure 1 Grain size distribution curves of test materials

508

509

510

511

512

513

514

515

516

517

518

519

520

(a)

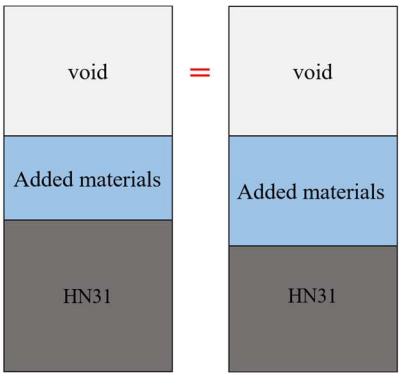

(b)

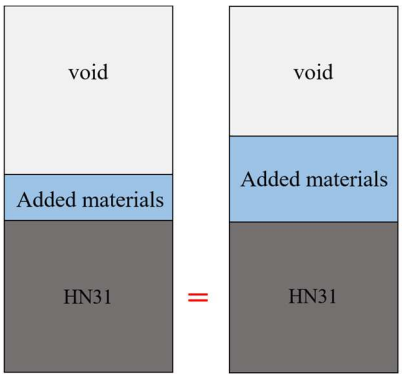

Figure 2 (a) Constant global void ratio; (b) constant density index of sand matrix (after Zhu [34])

(a) (b)

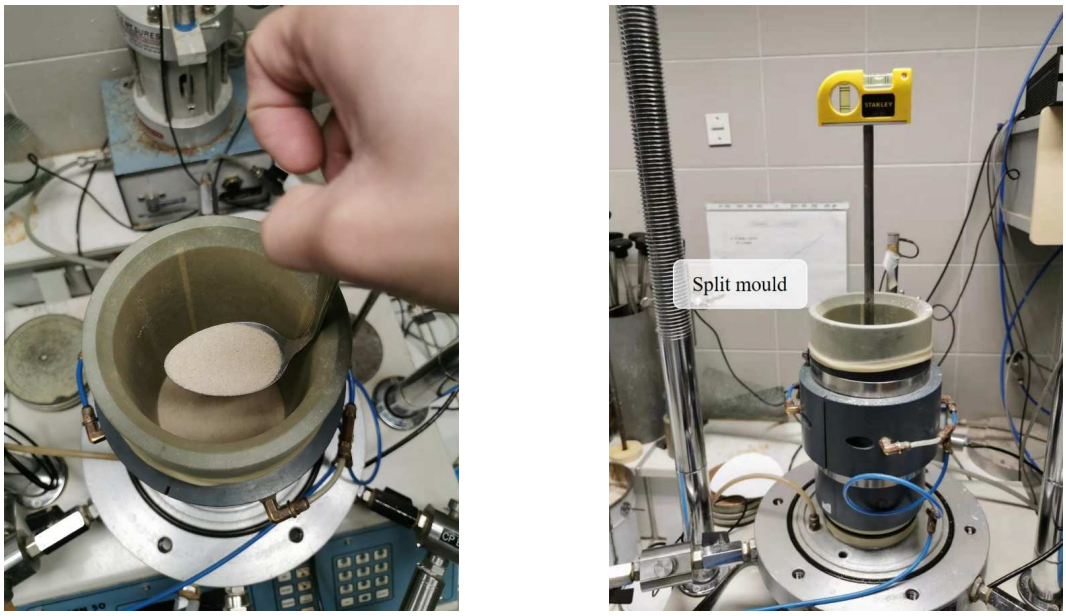

532 Figure 3 Dry tamping method (a) spooning the mixture into a split mould; (b) horizontality of each layer after slight
533 compaction

534

535

536

537

538

539

540

541

542

543

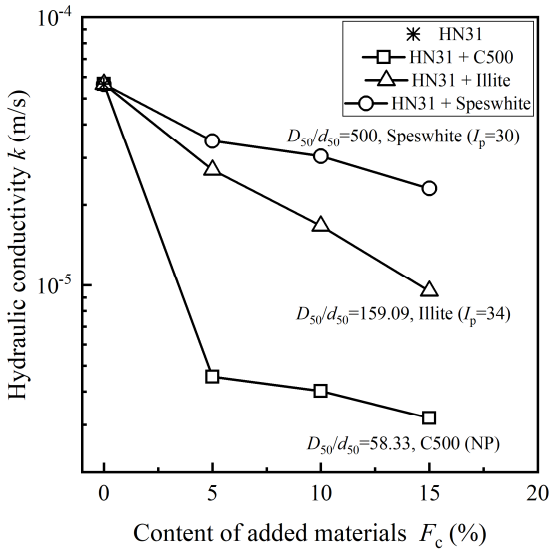

Figure 4 Effect of content of added materials F_c on the hydraulic conductivity k

(a) (b)

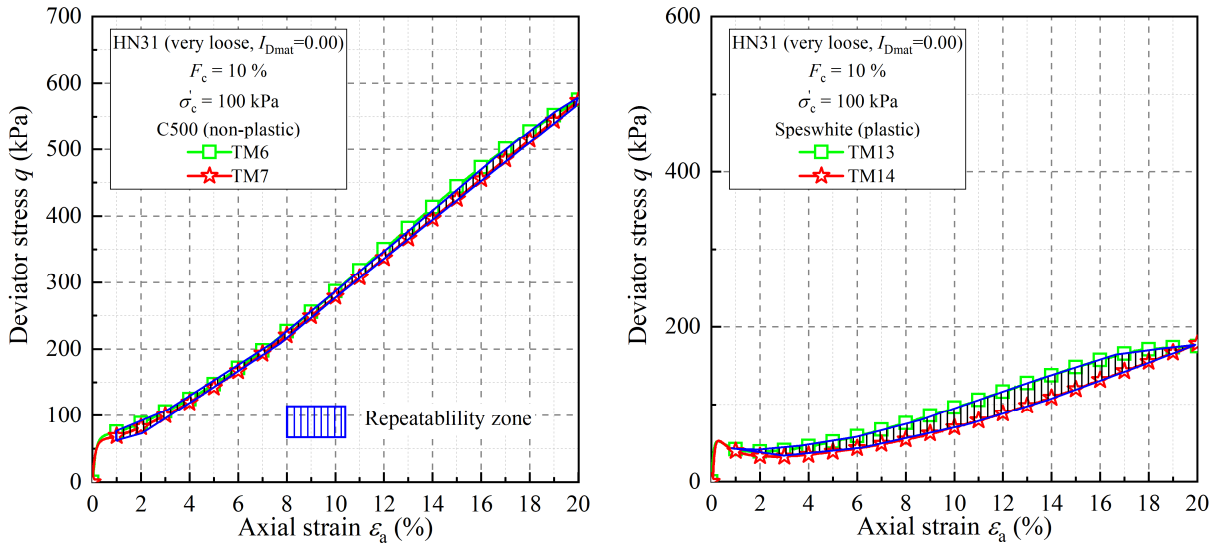

Figure 5 Repeatability tests under a confining pressure of 100 kPa in terms of stress-strain for (a) Sand-C500 mixture; (b) Sand-Speswhite mixture

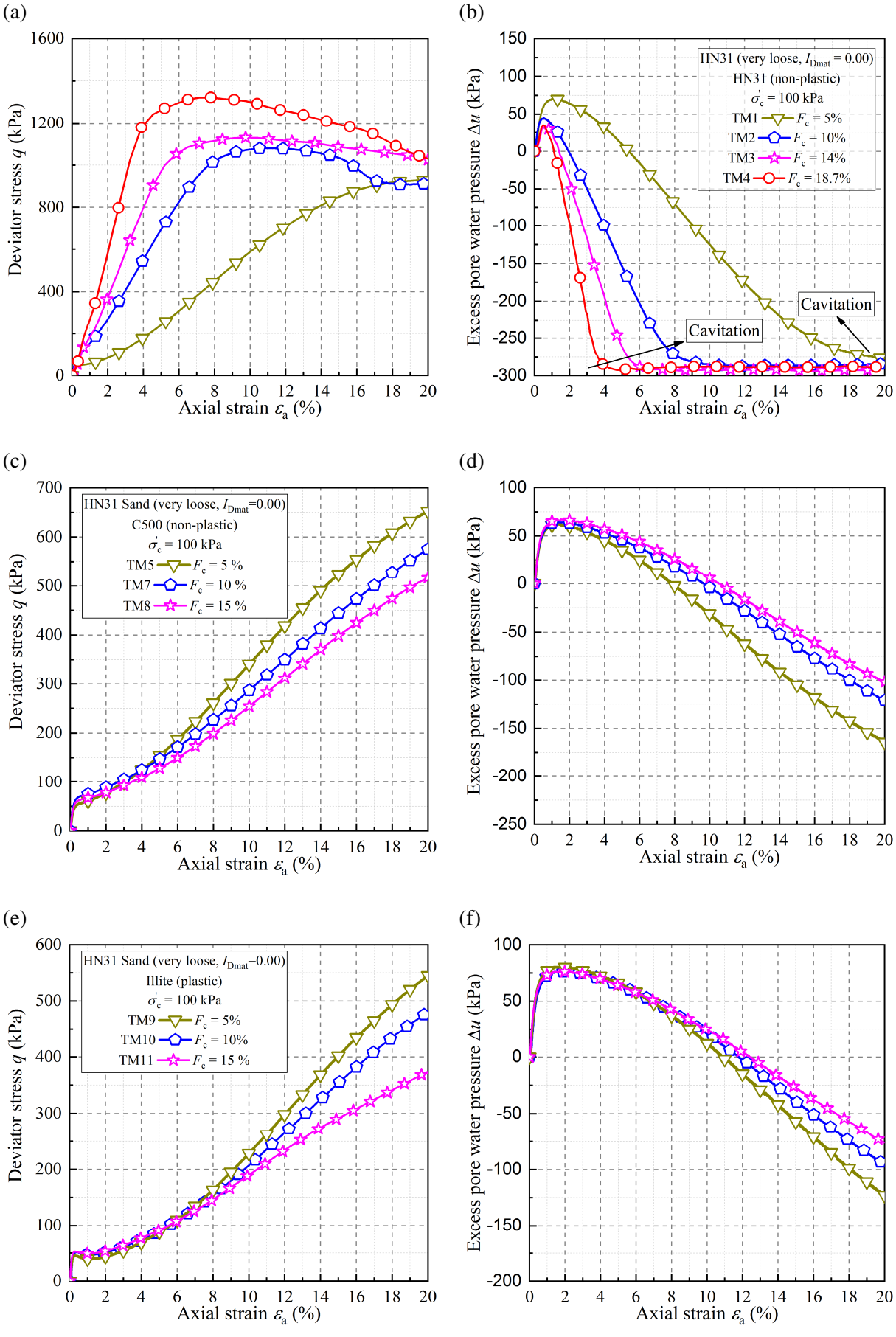
(a)
Deviator stress q (kPa)
Axial strain ε_a (%)
(b)
Excess pore water pressure Δu (kPa)
Axial strain ε_a (%)
HN31 (very loose, I_{Dmat} = 0.00)
HN31 (non-plastic)
σ_c' = 100 kPa
TM1 F_c = 5%
TM2 F_c = 10%
TM3 F_c = 14%
TM4 F_c = 18.7%
Cavitation
Cavitation
(c)
Deviator stress q (kPa)
Axial strain ε_a (%)
HN31 Sand (very loose, I_{Dmat}=0.00)
C500 (non-plastic)
σ_c' = 100 kPa
TM5 F_c = 5 %
TM7 F_c = 10 %
TM8 F_c = 15 %
(d)
Excess pore water pressure Δu (kPa)
Axial strain ε_a (%)
(e)
Deviator stress q (kPa)
Axial strain ε_a (%)
HN31 Sand (very loose, I_{Dmat}=0.00)
Illite (plastic)
σ_c' = 100 kPa
TM9 F_c = 5%
TM10 F_c = 10%
TM11 F_c = 15 %
(f)
Excess pore water pressure Δu (kPa)
Axial strain ε_a (%)

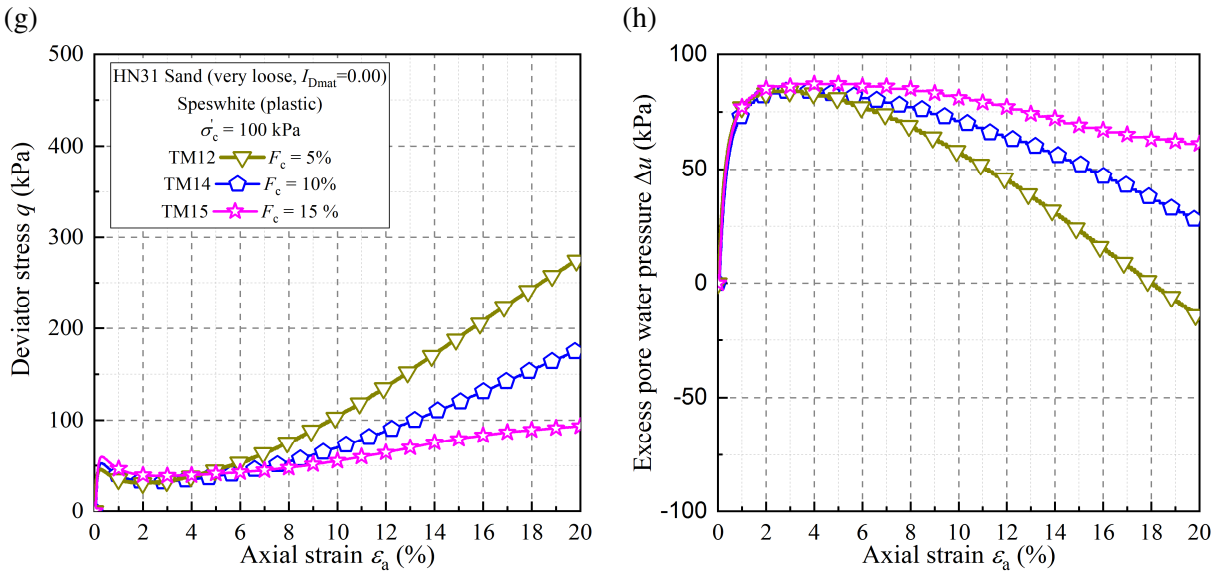

Figure 6 Effect of content of added materials on (a), (c), (e), (g) stress-strain curves; (b), (d), (f), (h) excess pore water pressure-strain curves

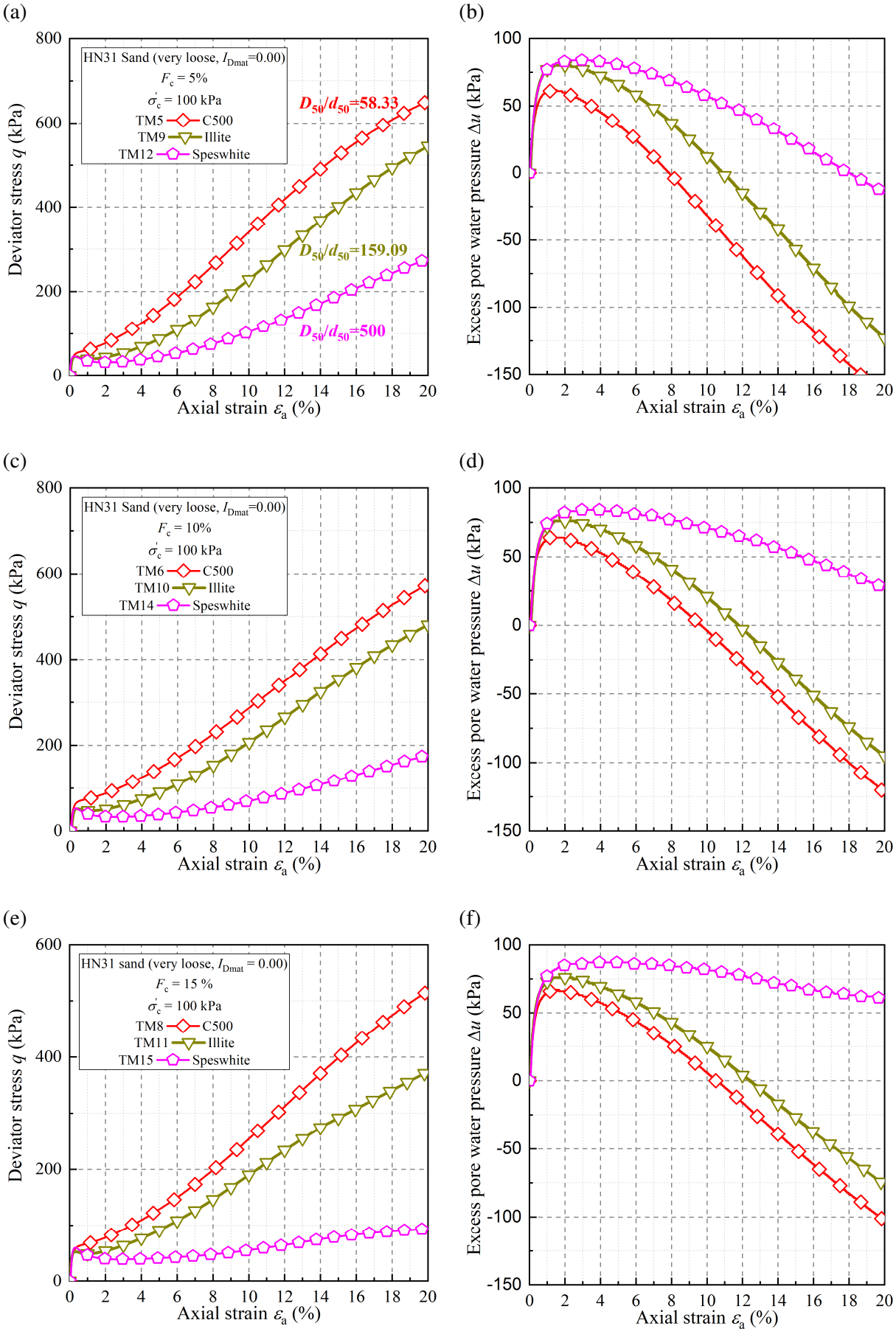
(a)
HN31 Sand (very loose, I_{Dmat}=0.00)
F_c = 5%
σ'_c = 100 kPa
TM5 C500
TM9 Illite
TM12 Speswhite
D_{50}/d_{50}=58.33
D_{50}/d_{50}=159.09
D_{50}/d_{50}=500
Deviator stress q (kPa)
Axial strain ε_a (%)
(b)
Excess pore water pressure Δu (kPa)
Axial strain ε_a (%)
(c)
HN31 Sand (very loose, I_{Dmat}=0.00)
F_c = 10%
σ'_c = 100 kPa
TM6 C500
TM10 Illite
TM14 Speswhite
Deviator stress q (kPa)
Axial strain ε_a (%)
(d)
Excess pore water pressure Δu (kPa)
Axial strain ε_a (%)
(e)
HN31 sand (very loose, I_{Dmat} = 0.00)
F_c = 15 %
σ'_c = 100 kPa
TM8 C500
TM11 Illite
TM15 Speswhite
Deviator stress q (kPa)
Axial strain ε_a (%)
(f)
Excess pore water pressure Δu (kPa)
Axial strain ε_a (%)

Figure 7 Effect of mean diameter ratio on (a), (c), (e) stress-strain curves; (b), (d), (f) excess pore water pressure-strain curves for mixtures at different F_c

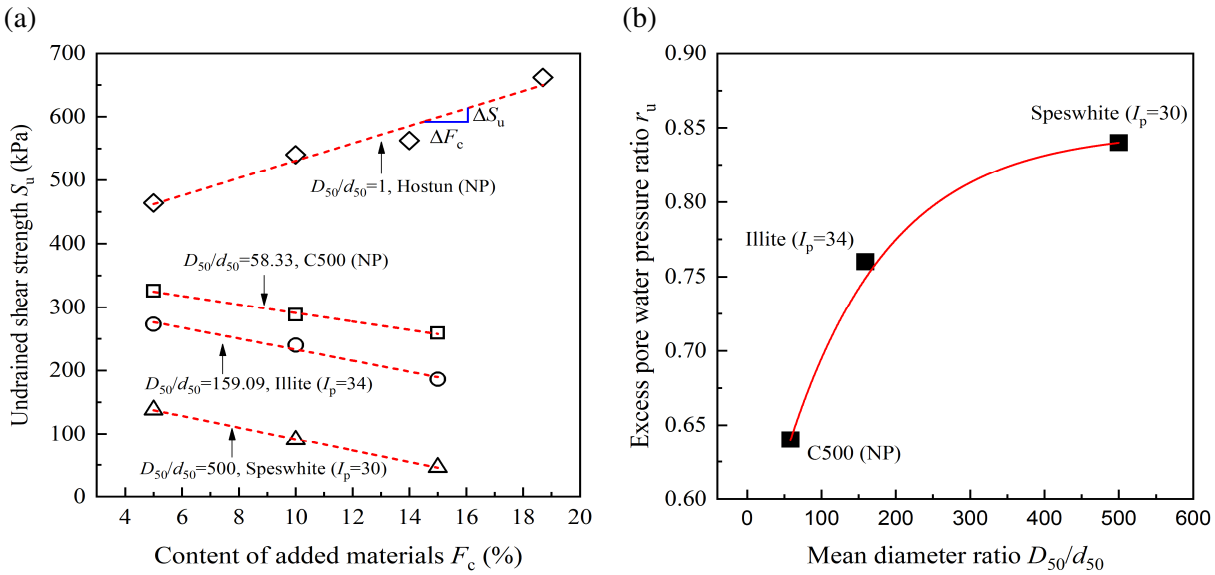

Figure 8 (a) Undrained shear strength versus content of added materials F_c; (b) excess pore water pressure ratio r_u versus mean diameter ratio D_{50}/d_{50}

605

606

(a) (b)

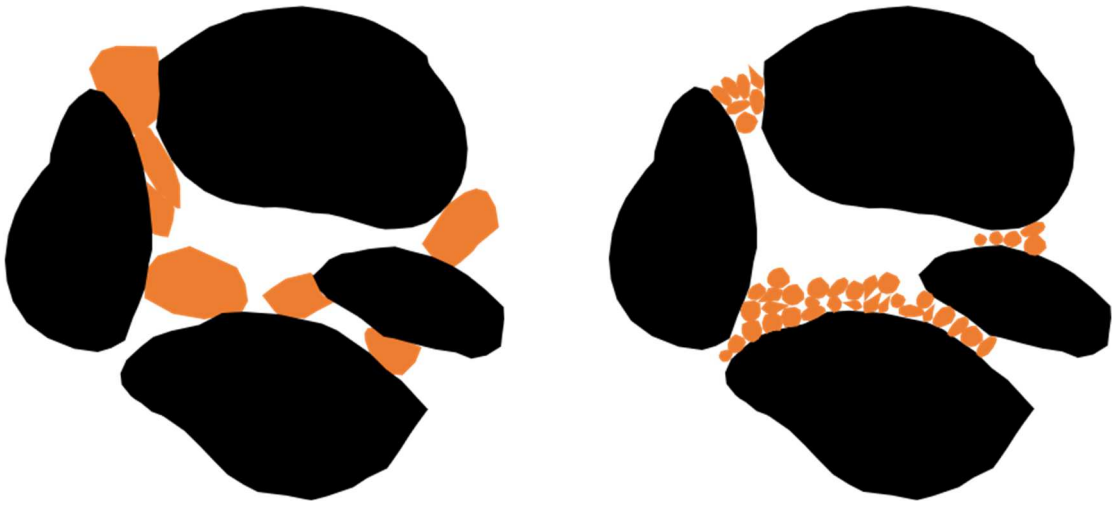

607 Figure 9 Schematic diagram of loose host sand containing added materials with (a) large-size grains; (b) small-size grains

608

609

610

611

612

613

614

615

616

617

618

619

620

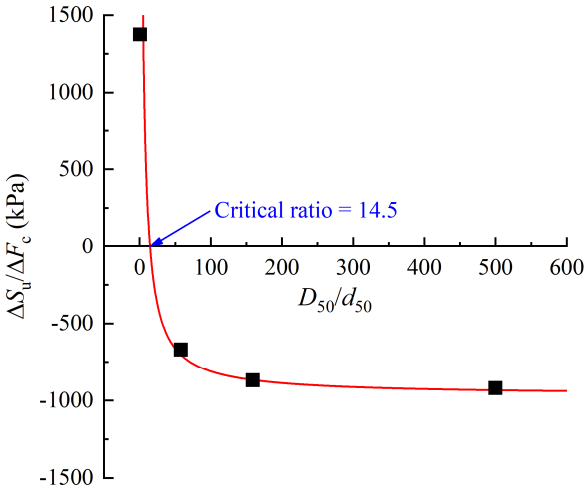

621

622 Figure 10 Variation of $\Delta S_u/\Delta F_c$ with D_{50}/d_{50}

623